Research Article Vol. 30, No. 3 / 31 Jan 2022 / Optics Express 4046
Optics EXPRESS

Laser energy prediction with ensemble neural networks for high-power laser facility

ZOU LU,[1,2] GENG YUANCHAO,[2] LIU GUODONG,[1,3] LIU LANQIN,[2] CHEN FENGDONG,[1] LIU BINGGUO,[1] HU DONGXIA,[2,4] ZHOU WEI,[2] AND PENG ZHITAO[2]

[1]*Harbin Institute of Technology, Harbin 150001, China*
[2]*Laser Fusion Research Center, China Academy of Engineering Physics, Mianyang 621900, China*
[3]*lgd@hit.edu.cn*
[4]*dongxia.hu@163.com*

Abstract: The energy accuracy of laser beams is an essential property of the inertial confinement fusion (ICF) facility. However, the energy gain is difficult to control precisely by traditional Frantz-Nodvik equations due to the dramatically-increasing complexity of the huge optical system. A novel method based on ensemble deep neural networks is proposed to predict the laser output energy of the main amplifier. The artificial neural network counts in 39 more related factors that the physical model neglected, and an ensemble method is exploited to obtain robust and stable predictions. The sensitivity of each factor is analyzed by saliency after training to find out the factors which should be controlled strictly. The identification of factor sensitivities reduces relatively unimportant factors, simplifying the neural network model with little effect on the prediction results. The predictive accuracy is benchmarked against the measured energy and the proposed method obtains a relative deviation of 1.59% in prediction, which has a 2.5 times improvement in accuracy over the conventional method.

1. Introduction

As a huge and complex high-power laser system, the Inertial Confinement Fusion (ICF) facility is expected to realize nuclear fusion for clean energy by bombarding the deuterium and tritium target simultaneously with hundreds of high-power laser beams [1–3]. To keep the uniformity of nucleus compression, the energy of every laser beam has to be controlled with extreme precision [4]. However, each of optical paths contains several sub-systems and large amounts of optical, electrical, and mechanical components [5,6]. Lots of factors increase the uncertainty of control and prediction. Traditionally, the output energy of the laser beams is predicted by analytical models and computer simulations. National Ignition Facility (NIF) has developed the Laser Performance Operation Model (LPOM) to predict the output energy of 192 beamlines in real-time [7,8], which is based on the Frantz-Nodvik (F-N) equation with diagnostic feedback data from historical experimental shots. With the aids of LPOM, NIF realizes energy control with 2-4% accuracy over a wide range from 0 to 25kJ [9,10]. The ICF facility in China has also built the Laser Performance Operation Simulation System (LPOSS) based on physical analytical models, which obtains a prediction accuracy of about 4% [11]. In reality, the simulations in ICF experiments contain simplifying assumptions. However, the dynamic coupling physical process of ICF involves many variables and responses, which is difficult for analytical model establishment. The simplified models lead to discrepancies between the prediction and experimental measurement.

A common approach is to use experimental data to set up an artificial neural network (ANN) as an accurate model, which is more consistent with the actual process. ANN is a connectionism model inspired by the biological neural network. It processes the received data and passes the processing results to the connected artificial neurons. ANN has a strong ability to learn

#447763 https://doi.org/10.1364/OE.447763
Journal © 2022 Received 9 Nov 2021; revised 5 Jan 2022; accepted 13 Jan 2022; published 24 Jan 2022

Optics EXPRESS

nonlinear mappings and complex representations. It has a wide range of applications not only in common fields as computer vision and natural language processing, but also in big science and computational fields [12–14]. As for the research of the Large Hadron Collider (LHC) experiments, the standard approaches have a limited capacity to solve the signal-versus-background classification problems [15]. A five-layer neural network is a powerful boost for learning complex nonlinear functions and searching for exotic particles with as much as 8% improvement [16]. To determine values of underlying parameters from measurements at the LHC, a multi-layer perceptron is trained with CMSSM as a toy model whose parameter space is manageable. It shows that ANNs can yield better and more reliable results with less computational effort than conventional minimization [17]. The scope of possibilities separating a single massive fat jet from QCD backgrounds is considerable, and a suite of dedicated taggers is not able to cover every possibility. A generic model-independent tagger using a neural network is developed and applied to signatures over a wide range of jet masses without sculpting the background distributions, which has a significant improvement [18]. Besides, ANNs can assist complex model development such as turbulence models. Supervised learning algorithms are used to build a representation of turbulence modeling source terms with large amounts of data from the Spallart-Almarams model. It reproduces the solutions with given observations of CFD solutions without knowing the actual model's structure, functional form, and coefficients, highlighting the potential and viability of data-driven approaches to aid complex model development [19]. As for Tokamak devices, a fully-connected ANN is adopted to improve the ideal magnetohydrodynamic no-wall limit component of the kinetic stability model in disruption event characterization and forecasting. It obtained encouraging results by testing against a set of experimentally stable and unstable discharges [20]. As for ICF, researchers use neural networks to explore high-dimensional design and simulation spaces [21–23]. Deep neural networks are used to learn the response of an expensive radiation hydrodynamics code over 9-dimensional parameter space. They then navigate parameter space to find implosions that optimize a combination of high neutron yield implosion robustness. To calibrate from low fidelity simulations to high fidelity ICF experiments, ANN is trained via transfer learning and essentially bootstraps the calibration process. It enables the creation of models more predictive of Omega experiments with minimal computational cost, which can be applied to search for new, optimal implosion designs [24]. In the view of above, ANNs have excellent ability to extract and analyze the relationship between measurable outputs and complicated inputs, which suffice as nonlinear models to represent and simulate complex physical processes. Meanwhile, neural networks have their inherent shortcomings, such as poor robustness, lack of interpretability, and poor compatibility.

In this study, based on the analysis of the experimental data in the main amplifier system of the ICF facility, we establish an ensemble neural network to predict the output energy of laser beams, which has a strong representation ability of the multivariable coupling and nonlinear process. The widely used simplified analytical model considers the energy gain as a stable inherent property of the amplifier system, and the output energy depends only on the input energy. However, in contrast to the conventional cognition, it has been observed that the measured data in 40 dimensions have a combined effect in the output which is difficult to decouple. We establish an artificial neural network to simulate the multivariable coupling process with neural nodes. As measured data cannot cover every physical possibility of the complicated system, we reduce the uncertainty of the output energy by weighted averaging. The proposed model is verified with the latest data of physical experiments and obtains excellent performance with an improvement of 60.9% in relative deviation. According to the prediction results, we further discuss the sensitivity of each factor and related physical explanations. The study investigates a deep learning model that will solve the prediction of laser energy with high-dimensional coupling parameters, which can be further applied to simulate and analyze of related complex optical systems and promote the development of optical systems.

Optics EXPRESS

2. Data collection and primary analysis

In the past three years, we carried out hundreds of physical experiments in the ICF facility in China and obtained a large amount of data on laser performance, facility status, and ambient status. For the main amplifier system, the laser beams from the pre-amplifier are injected into the cavity amplifier first and then oscillate following the red path, as shown in Fig. 1. It provides tens of thousands of times of energy gain by stimulated ions in pumped Nd: glass slabs. Based on the experience accumulated in the long-time operation, there are at least the following parameters that affect the output energy, the injected energy, pulse width, amount of Nd: glass slabs in cavity amplifier, time information of each trial shot which represents the immeasurable status of the main amplifier system (year, month, date, time and shot sequence within each day), ambient temperature and humidity.

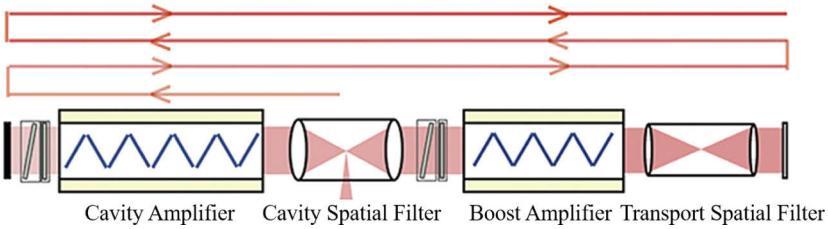

Fig. 1. Internal optical circuit and main modules of the main amplifier. Lasers inject into the main amplifier from the cavity spatial filter and transmit in the red line direction. Lasers pass through the cavity amplifier four times and the boost amplifier three times.

Aiming at the output energy of the main amplifier, we extract and sort 40 relevant data and plot them in Fig. 2. The different colors represent each experiment, and the ordinate represents the value of each parameter. The data of each shot are sorted according to the value of the input energy; that is to say, shots with darker colors have lower input energy, and the color of data points on the first ordinate is arranged as lighter to darker from top to bottom. Observing the last ordinate, which represents the output energy, the colors of data points are not following the input gradients but messed up. In the conventional energy prediction method, the amplification is described by Frantz-Nodvik (F-N) equation (more details are in Appendix A). It is a monotonic function that cannot accurately describe the non-monotonic variation of the energy amplification process.

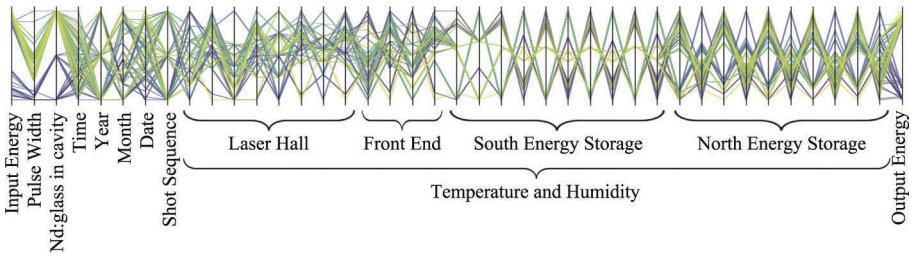

Fig. 2. Related data captured during operations.

Specifically, we select several typical factors and show their effects in Fig. 3. As for the effect of pulse width, wider pulse width brings greater energy amplification, shown in Fig. 3(a). Wider pulse width generates the gain recovery effect when the laser propagates as a pulse in the amplifier. The relaxation time, shorter than the time interval between multi-passes, causes the particle number reversal, making the output energy higher than expected. The ambient temperature and

Optics EXPRESS

humidity, shown in Fig. 3(b) and (c), influence the amplifying process as well. Humidity at the front end affect the properties of the fiber and change the spectrum, thus producing variations in the response of the gain distribution. The temperature and humidity of the north and south energy stores affect the efficiency and capacity of the capacitor charge and discharge, which can alter the pump light and gain performance and thus the output energy. Moreover, the state of the amplifier and the degree of component degradation are difficult to measure and evaluate, so we characterize them in terms of temporal characteristics, which impact the gain performance.

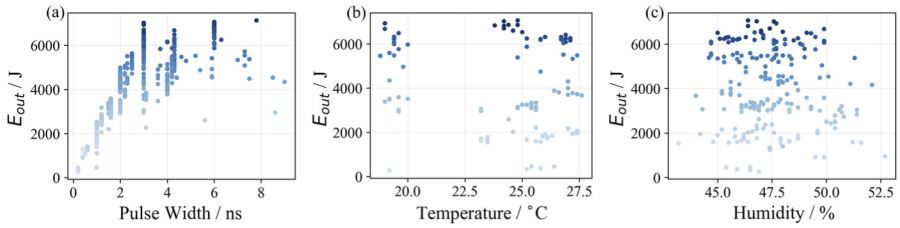

Fig. 3. Coupling effect of (a) pulse width, (b) temperature, and (c) humidity and input energy on output energy. The color shades of the data points indicate the magnitude of the input energy.

The data and analysis above show that the output energy is related to each of the 40 parameters, but the dynamic effects of 39 of which are ignored in the traditional prediction method with the F-N equation. Due to the high dimensions of parameters and the difficulty in measuring key parameters, it is not easy to describe the amplification process by traditional analytical methods. The coupling of observable parameters further increases the computation complexity exponentially. Thus, it is too complex to reveal the mechanism of the main amplifier through the analytical method, and it is necessary to adopt the data-driven approach with ANN models to solve the energy prediction problem efficiently and accurately.

3. Modeling and experimental verification

An artificial neural network (ANN) with two hidden layers of 100 neurons each is proposed to predict the output energy, representing the coupling process of 40 input features and mapping the physical amplification process to numerical process, shown in Fig. 4. Neurons in each layer are fully connected with those in the subsequent layer, values of which operate on a linear combination and a nonlinear activation, as $h^{(i)} = f^{(i)}\left(W^{(i)}h^{(i-1)} + b^{(i)}\right)$ for features $h^{(i)}$ in hidden layer i. Each input value is nonlinearly transformed into a representation of high-dimensional features with various weights, as Fig. 4(a), which can fit any function as long as the neural network has sufficient neurons. Multiple input features connect with all neurons in the subsequent layer and are coupled by the linear combination with a large matrix of weights to output features of each neuron to the next layer. The coupling between input parameters runs throughout the network, which has the ability to reproduce the nonlinear and multivariable coupling physical process well, shown in Fig. 4(b).

When we train the proposed ANN several times with measured data, fluctuating outputs are obtained due to local minima traps led by different optimization trajectories. An ensemble neural network (eANN) [25,26], composed of 10 sub neural networks with the same architecture and different initial parameters, is proposed to diminish the output fluctuation by calculating the weighted mean of the ten single outputs, shown in Fig. 5.

The optical system is too complex for experimental data to cover the infinite response and optimization trajectories during training. Thus, the numerical model is incapable of reproducing all physical possibilities, and inevitable random errors exist. The prediction results of ANNs

Optics EXPRESS

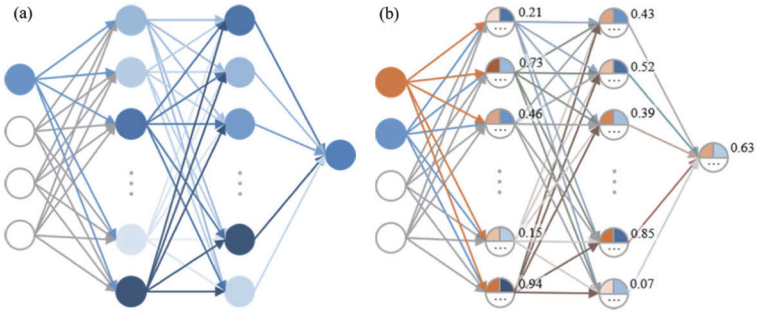

Fig. 4. The architecture of the three-layer artificial neural network. (a) The forward propagation of a single input feature. (b) The coupling between two input features during the forward propagation. The numbers represent the feature values output by each neural node.

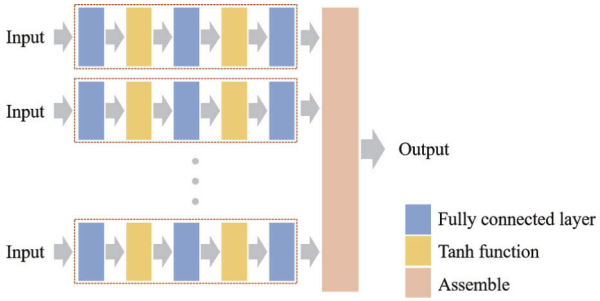

Fig. 5. The architecture of the ensemble neural network.

trained with randomly initialized parameters is a set of unequal-accuracy observation of the output energy $\hat{E}_1, \hat{E}_1, \ldots, \hat{E}_n$ with root mean square error (RMSE) $m_1, m_1, \ldots, m_n$. According to the error theory, the most probable value of the output energy is the weighted average of observations

$$\hat{E} = \frac{P_1\hat{E}_1 + P_2\hat{E}_2 + \cdots + P_n\hat{E}_n}{P_1 + P_2 + \cdots + P_n}, \tag{1}$$

where P_i is the weight of the observation i, $P_i = {m_0}^2/{m_i}^2$, and m_0 is the standard error of unit weight.

According to the error propagation formula of the linear function, the RMSE of the weighted mean of observations is

$$m_E = \sqrt{\left(\frac{P_1}{[P]}\right)^2 {m_1}^2 + \left(\frac{P_2}{[P]}\right)^2 {m_2}^2 + \cdots + \left(\frac{P_n}{[P]}\right)^2 {m_n}^2}, \tag{2}$$

where $[P] = P_1 + P_2 + \cdots + P_n$. Thereby, Eq. (2) can be reduced to

$$m_E = \frac{m_0}{\sqrt{[P]}}, \tag{3}$$

which is smaller than the RMSE of each observation $m_i = m_0/\sqrt{P_i}$. Thus, the method of weighted averaging can diminish error to predict output energy with higher precision.

As for ANN, the output performance is evaluated by a loss function, precisely smooth L1 loss in this research, which guarantees fast convergence in optimization and less sensitivity to

Optics EXPRESS

observations with significant errors and is defined as

$$L = \begin{cases} \frac{1}{2n}\sum_{i=1}^{n}(\hat{y}_i - y_i)^2, & |\hat{y}_i - y_i| < 1 \\ \frac{1}{n}\sum_{i=1}^{n}\left(|\hat{y}_i - y_i| - \frac{1}{2}\right), & otherwise \end{cases}, \tag{4}$$

where n is the number of training samples, $\hat{y}_i$ is the output prediction of the network, and y_i is the actual value of output energy measured in experiments.

We assemble these ten individual ANNs and obtain the eANN by averaging with weights according to Eq. (2). The weight P_i of each sub-ANN is the reciprocal of loss, which is mean square error (MSE) during the later stages of training.

In order to construct datasets for training and testing, historical data measured during operation within three years are arranged in chronological order. The former 90% data (538 samples) form the training dataset, which guides the ANNs to learn appropriate parameters. The other 10% latest data (52 samples) form the testing dataset, which is regarded as future data and benchmark to evaluate the performance of the energy prediction model. Each sub-ANN is trained by Adagrad optimization with random initialization for 1000 epochs unless the output meets the specified accuracy requirements or the output performance gets persistent deterioration.

The prediction results of ten trained sub-ANNs are unequal-accuracy and varying, as Fig. 6(a) shows. The blue pentagrams on the blue regression line are ground truth, and stars of various colors represent the predictions of each ANN. Cyan stars (sANN9) have more minor errors while gray stars (sANN7) have significant errors, and some samples have unacceptably large residuals. The single ANN model has poor robustness and repeatability. Conversely, the prediction results of eANN, shown as Fig. 6(b), are all on the regression line with minor errors, which perform better than any of the sub-ANNs. The eANN model possesses increased stability, high accuracy, and strong generalization ability.

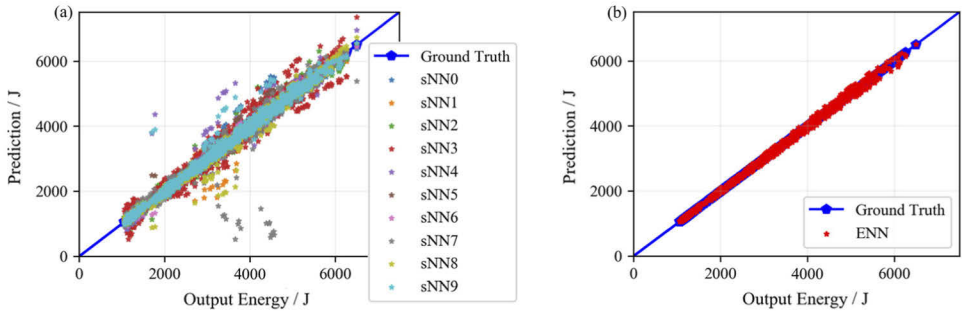

Fig. 6. Regression performances of (a) ten trained sub-ANNs, (b) eANN.

To validate the effectiveness of the proposed eANN, we test the trained eANN with the testing dataset, which is regarded as experiments in the future. The testing results are evaluated by RMSE and mean absolute relative deviation (MARD). The performance of the conventional method by resolving the F-N equation, single ANN (sANN), and eANN for two beamlines are listed in Table 1. The results of sANNs with the best performance and worst performance are both listed. The prediction results of sANNs outperform the F-N equation. The proposed eANN method outperforms the others with the most minor errors and the prediction accuracy is improved by 2.5 times compared with the conventional F-N equation model.

More details about the prediction performances are obtained by observing the relative deviation in chronological order. As shown in Fig. 7(a), The fluctuation trends of the prediction deviations are similar for both methods, but eANN is significantly smoother. The prediction deviation of

Optics EXPRESS

Table 1. Prediction performances of each method with data from various beams.

Method		RMSE				MRAD			
		F-N	Worst-sANN	Best-sANN	eANN	F-N	Worst-sANN	Best-sANN	eANN
Beam1	Training	256.81	140.61	75.46	**63.18**	4.13	2.82	1.53	**1.20**
	Testing	215.71	152.56	93.49	**79.50**	4.07	3.08	1.86	**1.59**
Beam2	Training	241.00	218.55	104.77	**71.55**	4.70	10.94	4.43	**2.97**
	Testing	221.89	303.30	147.73	**108.68**	6.68	9.94	4.69	**2.60**

eANN is mostly under 4% in the whole test set, while the deviation of the traditional calculation method using the F-N equation is much larger. In addition, as the amount of future experiments increases, the deviation of the traditional method becomes larger, while the deviation of eANN remains within a smaller range because it has captured the influence of time and ambient factors. It indicates that the eANN method is able to predict the output energy more consistently and accurately. The histograms of relative deviation with both methods are shown in Fig. 7(b), in which the mean relative deviation of the network model is −0.52, and the variance is 2.42, while the mean relative deviation of the traditional method is 4.84 and the variance is 3.01. It illustrates that the distribution of the deviations of the eANN method is more concentrated and distributed around 0, while the distribution of the deviations of the classical method is wider and biased towards positive. Most of the predictions of the classical method are high biased and less accurate than those of the eANN method. In addition, even if the parameters are fine-tuned so that the F-N equation fits the actual input-output curve as closely as possible, the deviation of prediction results is larger than the network prediction results. Therefore, the proposed network model is effective for laser energy prediction.

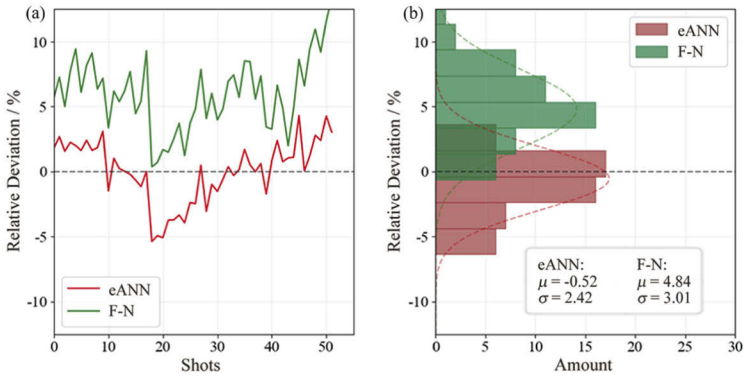

Fig. 7. Relative standard deviation (a) curves and (b) histograms of conventional F-N method and ensemble ANN method in chronological order.

4. Discussions

To further explore the internal mechanism of the 40 input features in the main amplifier process, we calculate and visualize their sensitivity to observe their influence on the output energy, which is called the saliency in regression analysis. The saliency is calculated by the partial differential of each sub-network, which is deduced as

$$\frac{\partial y_i}{\partial X} = W_1{}^{\mathsf{T}} \cdot \left\{ W_2{}^{\mathsf{T}} \cdot \left[W_3{}^{\mathsf{T}} \odot \left(I_{h_2} - h_2 \odot h_2 \right) \right] \odot \left(I_{h_1} - h_1 \odot h_1 \right) \right\}, \tag{5}$$

Optics EXPRESS

where I_{h_k} is a matrix with the same size as h_k and the elements of I are all 1. y_i is the output of the ith sub-network and X is the input vector with 40 elements. W_j is the weight matrix of the jth layer in the neural network, and h_k is the output of the kth layer. The h_1 and h_2 are calculated by

$$h_1 = \tanh\left(W_1 \cdot X + b_1\right), \tag{6}$$

$$h_2 = \tanh\left(W_2 \cdot h_1 + b_2\right). \tag{7}$$

The saliency result of each sample is a vector with the size of 40×1. Each element represents the effect of the corresponding argument on the output energy. Each sample leads to a different saliency vector for the entire dataset. Nevertheless, different samples of the same element have similar statistical characteristics. Their statistical results are shown in the box diagram in Fig. 8 . The top and bottom edges of the vertical line represent the maximum and minimum values, and the upper and lower edges of the rectangular box represent the upper and lower quartiles, respectively. The orange line in the middle of the rectangular box is the median of the saliency results.

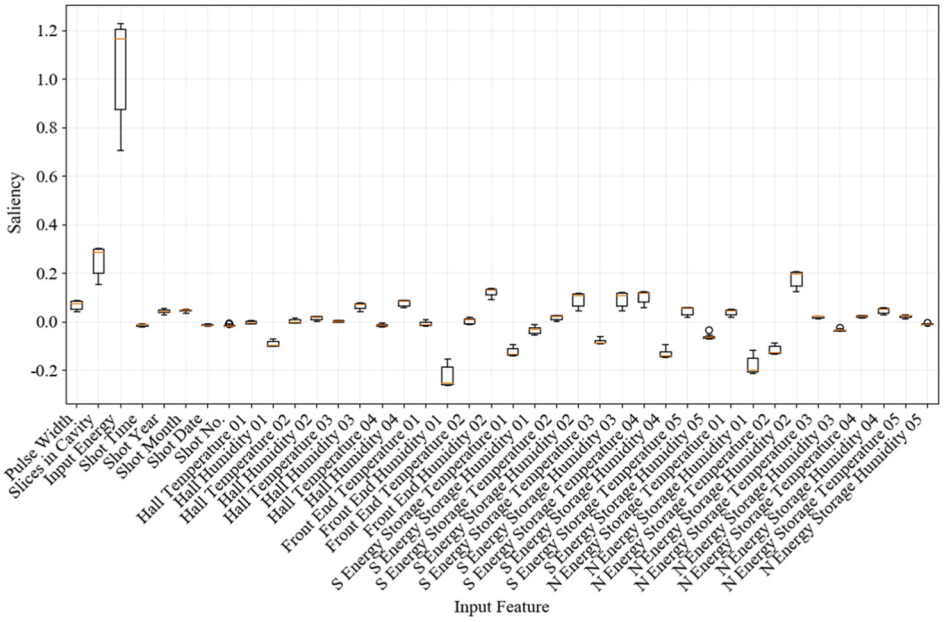

Fig. 8. The saliency results of the output energy with respect to each of 40 input features.

In the significance chart, the features with saliency closer to zero have minor sensitivity. The third input feature, input energy, has the largest positive saliency, which affects the output energy significantly. The second input feature, the amount of Nd: glass slabs in the cavity amplifier, also has a significant positive saliency value and positive correlation effect on the output energy. The saliency results are consistent with the existing physical models and empirical knowledge (analyzed in Section 2). In particular, the input energy and slices in the cavity directly and powerfully affect the output energy. The year and month of shots are along with the upgrade and degradation of the facility. Environmental temperature and humidity affect the charging and discharging efficiency. They all affect the energy gain to varying degrees, but no physical model has yet to describe their relationship analytically.

The correlations of these factors are analyzed and shown in the heat map as Fig. 9. The larger the absolute value is, the stronger correlation they have. The temperature, as well as the

Optics EXPRESS

humidity, in the same building, has a strong correlation. Thus, only one feature among the similar characteristics needs to be preserved.

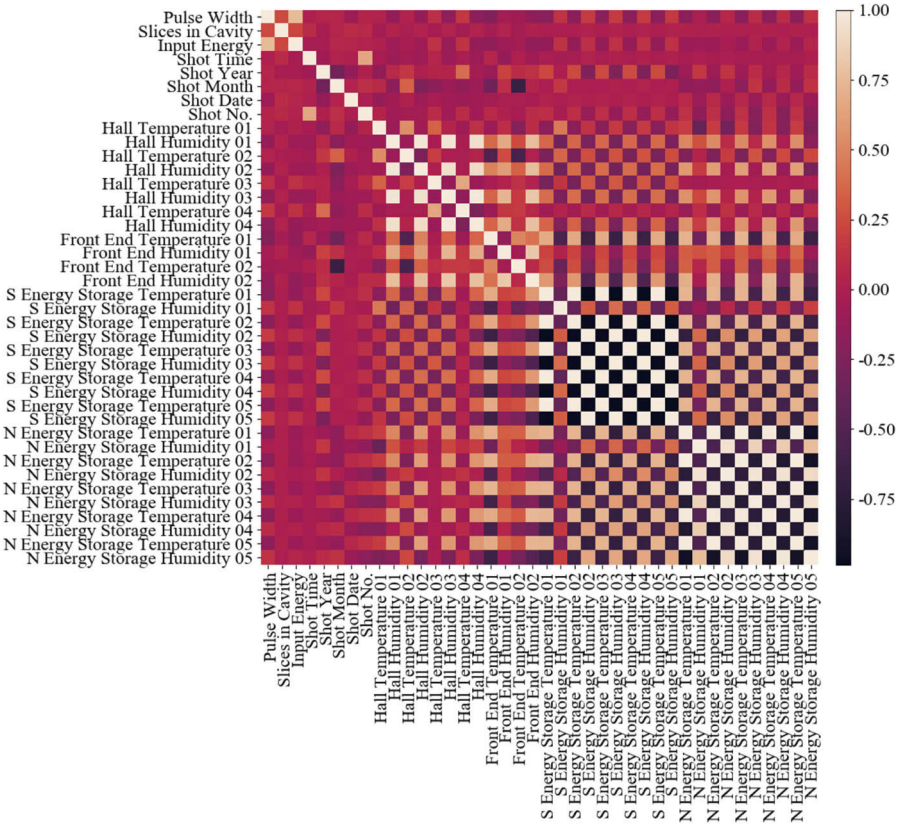

Fig. 9. Correlation of 40 arguments of the output energy.

With redundancy removal, a new input vector with 22 selected features is formed and used to train the network again. For beam line 1, the relative deviation of prediction is 2.08%, and for beam line 2, it is 2.84%. The saliency results of the newly trained model with the lightweight

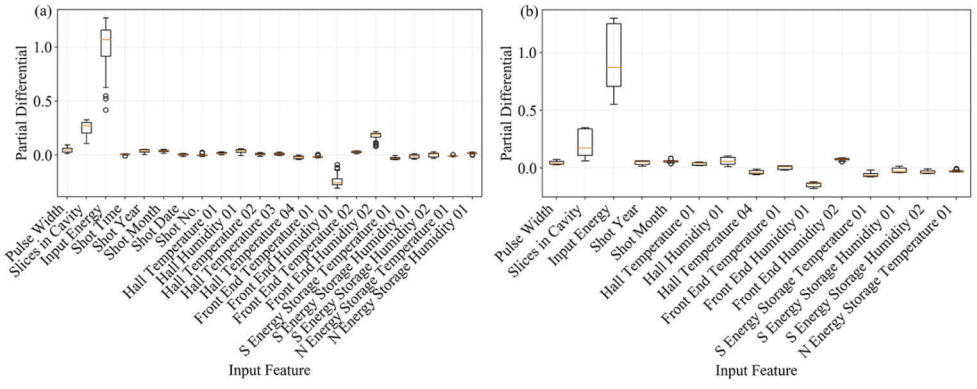

Fig. 10. The saliency results of the output energy to each of (a) 22 input features and (b) 15 input features.

Optics EXPRESS

dataset are shown in Fig. 10. The partial derivatives are consistent with the original model of 40 input features. The saliency results' value and range of some salient features remain unchanged, such as pulse width, amount of amplifier, and input energy. Meanwhile, the simplified temperature and humidity features also retain their sensitivity, which shows the stability of the eANN model.

Moreover, 15 of the 22 input features with great sensitivity are selected to simplify the input features. The network is further lightened to accelerate the computing speed. After training, the network prediction performance remains well, with a testing deviation of 2.48%. The prediction and saliency results of models with 40, 22, and 15 input features are similar, with little change. It illustrates that the proposed eANN model has strong stability and repeatability.

5. Conclusions

In this work, an ensemble ANN is presented to predict the laser output energy of the main amplifier in a high-power ICF facility. We select 40 factors based on our operational experience and present an ANN model to characterize their coupling effects on the complex gain process. An ensemble ANN obtained by integrating ten independent ANNs improves the accuracy and robustness of prediction. The saliency of all input features is further analyzed, which is consistent with the empirical knowledge. Based on the correlation and saliency analysis, we choose 15 factors with the most significant sensitivity, which need extra attention in operation. After retraining the light-weighted eANN model, the prediction performance remains well, proving the credibility of analysis and the selected factors. The proposed eANN is benchmarked with recent experimental data measured at the facility, with a relative deviation in prediction of 1.59% and a 2.5 times accuracy improvement over the conventional method. The proposed method provides a connectionism model for energy prediction and indicates vital variables that need attention and management. We explore the potential of ANN as an enhancement or replacement for traditional models of complex physical processes. Our results investigate the viability of neural network approaches to further physical model development.

Appendix A. Details of Frantz-Nodvik equation

The amplification process is described by the Frantz-Nodvik (F-N) equation which is a solution of the laser rate equations [27], expressed as

$$E_{out} = E_s \ln\left\{1 + \left[\exp\left(\frac{E_{in}}{E_s}\right) - 1\right] G_0\right\}, \tag{8}$$

where, E_{out} is the output energy, E_{in} is the input energy which is represented as $E_{in} = c\phi_0 t_p h\nu$, E_s is the saturation flux which is defined as $E_s = h\nu/\gamma\sigma$, and G_0 is the small-signal gain which is defined as $G_0 = \exp(n\sigma l)$. In the formulae, ϕ_0 is the initial photon density, t_p is the duration of a square pulse, σ is the stimulated emission cross section, n is the inversion population density, and l is the length of the laser amplifier.

The conventional energy prediction is conducted by resolving Eq. (8) with data over a historical period to obtain appropriate E_s and G_0 . However, the prediction result is not accurate enough due to the following assumptions of the physical model.

Firstly, the temporal shape of the incident pulse is assumed to be rectangular when resolving the laser rate equations. However, in ICF experiments, incident power pulses are diverse and are commonly exponential super-Gaussian pulses with lower rising and higher falling parts. The solutions of rate equations based on pulses in experiments differ from Eq. (8), so the F-N equation cannot describe the output power waveform and energy accurately. Secondly, when establishing the rate equation, the amplifier is considered an equivalent large single-pass amplifier, but the laser pulse is multi-pass amplified in the facility. When the time interval is larger than

Optics EXPRESS

the relaxation time of the lower laser level in the four-level system, the regenerated population inversion produces the gain recovery effect. The F-N equation can only represent this process approximately.

Additionally, the F-N equation is established for the ideal operating environment. However, the amplifying characteristics decrease slowly with time, caused by the degradation of electronic and optical components. Slight changes in environmental parameters also produce minor disturbances of the amplifying capability. E_s and G_0 obtained by resolving the F-N equation with historical trial data are constants, yet they are variables that change along with the environmental disturbances. In other words, the prediction model of the F-N equation is designed in the ideal condition as $E_{out} = f_{FN}(E_{in}, E_s, G_0)$. However, due to the time-varying characteristics, the prediction model is $E_{out} = f_{FN}[E_{in}, E_s(t), G_0(t)]$ in operation. Therefore, data over different historical periods correspond to different solutions, as shown in Fig. 11. E_s and G_0 are solved with 20 and 30 historical samples and obtain different results. The results with more historical samples are smoother but have less capability to represent the time-varying characteristics.

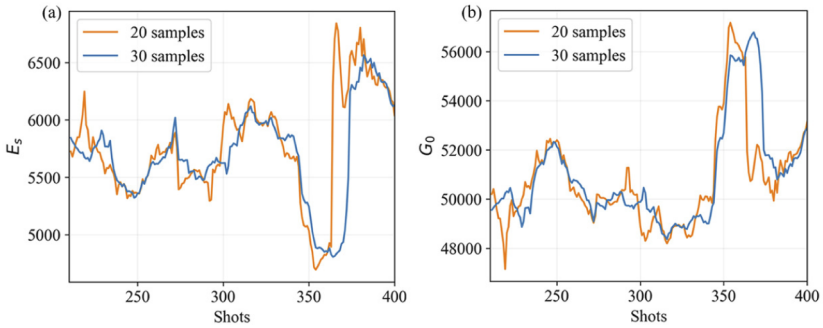

Fig. 11. (a) Saturation flux and (b) small-signal gain of the main amplifier varies with operations with different trial data.

Disclosures. The authors declare no conflicts of interest.

Data availability. Data underlying the results presented in this paper are not publicly available at this time but may be obtained from the authors upon reasonable request.

References

1. B. Canaud, F. Garaude, P. Ballereau, J. Bourgade, C. Clique, D. Dureau, M. Houry, S. Jaouen, H. Jourdren, and N. Lecler, "High-gain direct-drive inertial confinement fusion for the laser mégajoule: recent progress," Plasma Phys. Controlled Fusion **49**(12B), B601–B610 (2007).
2. E. I. Moses, J. D. Lindl, M. L. Spaeth, R. W. Patterson, R. H. Sawicki, L. J. Atherton, P. A. Baisden, L. J. Lagin, D. W. Larson, and B. J. MacGowan, "Overview: Development of the national ignition facility and the transition to a user facility for the ignition campaign and high energy density scientific research," Fusion Sci. Technol. **69**(1), 1–24 (2016).
3. W. Zheng, X. Wei, Q. Zhu, F. Jing, D. Hu, J. Su, K. Zheng, X. Yuan, H. Zhou, W. Dai, W. Zhou, F. Wang, D. Xu, X. Xie, B. Feng, Z. Peng, L. Guo, Y. Chen, X. Zhang, L. Liu, D. Lin, Z. Dang, Y. Xiang, and X. Deng, "Laser performance of the SG-III laser facility," High Power Laser Sci. Eng. **4**, e21 (2016).
4. C. C. Kuranz, H.-S. Park, C. M. Huntington, A. R. Miles, B. A. Remington, T. Plewa, M. R. Trantham, H. F. Robey, D. Shvarts, and A. Shimony, "How high energy fluxes may affect rayleigh–taylor instability growth in young supernova remnants," Nat. Commun. **9**(1), 1564 (2018).
5. M. L. Spaeth, K. Manes, D. Kalantar, P. Miller, J. Heebner, E. Bliss, D. Spec, T. Parham, P. Whitman, and P. Wegner, "Description of the NIF laser," Fusion Sci. Technol. **69**(1), 25–145 (2016).
6. B. M. Van Wonterghem, S. J. Brereton, R. F. Burr, P. Folta, D. L. Hardy, N. N. Jize, T. R. Kohut, T. A. Land, and B. T. Merritt, "Operations on the national ignition facility," Fusion Sci. Technol. **69**(1), 452–469 (2016).
7. G. Brunton, A. Casey, M. Christensen, R. Demaret, M. Fedorov, M. Flegel, P. Folta, T. Frazier, M. Hutton, and L. Kegelmeyer, "Control and information systems for the national ignition facility," Fusion Sci. Technol. **69**(1), 352–365 (2016).

Optics EXPRESS

8. M. Shaw, R. House, W. Williams, C. Haynam, R. White, C. Orth, and R. Sacks, "Laser performance operations model (LPOM): A computational system that automates the setup and performance analysis of the national ignition facility," J. Phys.: Conf. Ser. **112**(3), 032022 (2008).
9. M. L. Spaeth, K. R. Manes, M. Bowers, P. Celliers, J.-M. D. Nicola, P. D. Nicola, S. Dixit, G. Erbert, J. Heebner, and D. Kalantar, "National ignition facility laser system performance," Fusion Sci. Technol. **69**(1), 366–394 (2016).
10. M. S. Hutton, S. Azevedo, R. Beeler, R. Bettenhausen, E. Bond, A. Casey, J. Liebman, A. Marsh, T. Pannell, and A. Warrick, "Experiment archive, analysis, and visualization at the national ignition facility," Fusion Eng. Des. **87**(12), 2087–2091 (2012).
11. J. Su, W. Wang, J. Feng, Z. Peng, and X. Zhang, "The code SG99 for high-power laser propagation and its applications," in *High-Power Lasers and Applications III*, vol. 5627 (International Society for Optics and Photonics, 2005), pp. 527–531.
12. K. Albertsson, D. Anderson, D. Kcira, H. Newman, and J. R. Vlimant, "Machine learning in high energy physics community white paper," J. Phys.: Conf. Ser. **1085**, 022008 (2018).
13. P. Baldi, K. Cranmer, T. Faucett, P. Sadowski, and D. Whiteson, "Parameterized machine learning for high-energy physics," arXiv preprint arXiv:1601.07913 (2016).
14. B. K. Spears, J. Brase, P.-T. Bremer, B. Chen, J. Field, J. Gaffney, M. Kruse, S. Langer, K. Lewis, R. Nora, J. L. Peterson, J. J. Thiagarajan, B. V. Essen, and K. Humbird, "Deep learning: A guide for practitioners in the physical sciences," Phys. Plasmas **25**(8), 080901 (2018).
15. M. Abdughani, J. Ren, L. Wu, J.-M. Yang, and J. Zhao, "Supervised deep learning in high energy phenomenology: a mini review," Commun. Theor. Phys. **71**(8), 955 (2019).
16. P. Baldi, P. Sadowski, and D. Whiteson, "Searching for exotic particles in high-energy physics with deep learning," Nat. Commun. **5**(1), 4308 (2014).
17. N. Bornhauser and M. Drees, "Determination of the cmssm parameters using neural networks," Phys. Rev. D **88**(7), 075016 (2013).
18. J. Aguilar-Saavedra, J. Collins, and R. K. Mishra, "A generic anti-qcd jet tagger," J. High Energy Phys. **2017**(11), 163 (2017).
19. B. D. Tracey, K. Duraisamy, and J. J. Alonso, "A machine learning strategy to assist turbulence model development," in *53rd AIAA Aerospace Sciences Meeting*, (2015), p. 1287.
20. A. Piccione, J. W. Berkery, S. A. Sabbagh, and Y. Andreopoulos, "Physics-guided machine learning approaches to predict the ideal stability properties of fusion plasmas," Nucl. Fusion **60**(4), 046033 (2020).
21. R. Nora, J. L. Peterson, B. K. Spears, J. E. Field, and S. Brandon, "Ensemble simulations of inertial confinement fusion implosions," Stat. Analysis Data Min. **10**(4), 230–237 (2017).
22. J. L. Peterson, K. D. Humbird, J. E. Field, S. T. Brandon, S. H. Langer, R. C. Nora, B. K. Spears, and P. T. Springer, "Zonal flow generation in inertial confinement fusion implosions," Phys. Plasmas **24**(3), 032702 (2017).
23. K. D. Humbird, J. L. Peterson, and R. G. McClarren, "Parameter inference with deep jointly informed neural networks," Stat. Analysis Data Mining: The ASA Data Sci. J. **12**(6), 496–504 (2019).
24. K. D. Humbird, J. L. Peterson, B. Spears, and R. McClarren, "Transfer learning to model inertial confinement fusion experiments," IEEE Trans. Plasma Sci. **48**(1), 61–70 (2020).
25. S. Fort, H. Hu, and B. Lakshminarayanan, "Deep ensembles: A loss landscape perspective," arXiv preprint arXiv:1912.02757 (2019).
26. Leo Breiman, "Bagging predictors," Mach. Learn. **24**(2), 123–140 (1996).
27. W. Koechner, *Solid-state laser engineering*, vol. 1 (Springer, 2013).